MORPHING CONCEPT OF UAVS OF THE SWEPT FLYING WING

Vasile PRISACARIU[1], Ionică CÎRCIU[2], Mircea BOŞCOIANU[2]
[1] Transilvania University of Brasov, Romania
[2] "Henri Coandă" Air Force Academy of Brasov, Romania

Abstract. A special class of unmanned air vectors is the flying wings, which are to be found in the areas of interest to the same extent as the conventional design aircraft. The tailless design of unmanned aircraft brings compact geometry and maneuverability advantages with generation of 3D evolutions. Although the benefits of the morphing concept are highlighted from the aerodynamic point of view, the technical achievements are still a critical issue. This article aims at analyzing the influence of constructive twist and of twist morphing on the performance of swept flying wings.

Keywords: UAS, swept flying wing, morphing wing, aerodynamic analysis

1. Introduction

Morphing is the ability to change shape (according to Webster's dictionary). The words "transform" and "morphing" are actually forms of the word "metamorphosis", which derives from the Greek "meta" (to change) and "morfe" (shape). It is a description of the ability to change the shape or geometry of bodies and wings for increased maneuverability as well as for a stable flight in a multitude of ambient conditions [1].

The concept of morphing was used with the advent of non-motorized aircraft. More precisely when Otto Lilienthal (1848-1896) used wing morphing to pilot his gliders and the Wright brothers (1903) applied the biological principles of the flight to change the aerodynamic characteristics of a plane through changing the shape of the wing and through the structural deformation technique by means of cables. Romanian and international aviation pioneers (Wright brothers, Traian Vuia) used similar solutions to build their airplanes, see Figures 1 and 2 [2, 3].

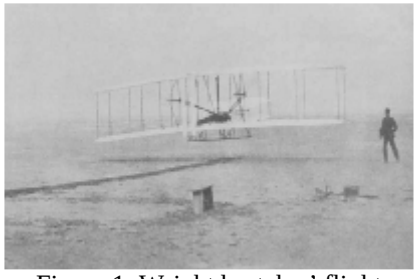

Figure 1. Wright brotehrs' flight

Morphing aircraft give the advantage of changing shape during flight for performance optimization in accordance with mission requirements or a flight stage. Although the benefits of the morphing concept are obvious from the aerodynamic point of view, the technical achievements are still a critical issue.

Figure 2. Traian Vuia's airplane

The tailless design of unmanned aircraft brings compact geometry and maneuverability advantages with generation of 3D evolutions. Although the benefits of the morphing concept are highlighted from the aerodynamic point of view, the technical achievements are still a critical issue mainly in what concerns the morphing command and control of load-lifting surfaces.

2. Current morphing concepts and research

The hyper-elliptical wing was developed by NASA Langley Research Center (Figure 3), which conducted a study on such HECS (Hyper-elliptic cambered span) wings as part of the Morphing Project within Vehicle Systems Technology Program [4, 12, 13].

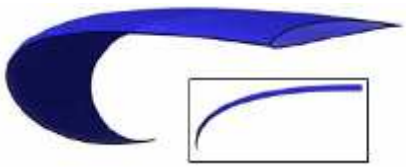

Figure 3. HECS wing

Extreme 3D Morphing, with modification of the wing end on an unmanned motor-glider within the Sky Walker project financed by DARPA, [5] was used in exploiting thermal currents through increased maneuverability due to the morphing of the wing tips (about 10% of span), see Figure 4.

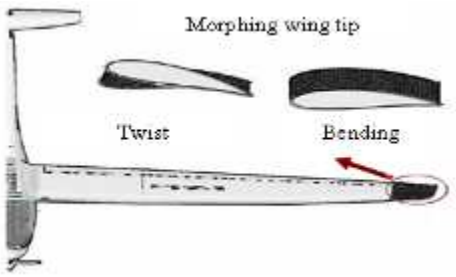

Figure 4. Morphing Sky Walker [5]

Multi-point 3D morphing (multi-servomotors) with symmetrical\/asymmetrical changes of the shape of the wing to control the vector; it is developed within the University of Florida Center for Micro Air Vehicles and Oregon State University, see Figure 5 [6].

Figure 5. Multi-point 3D morphing [6]

3. Theory

3.1. Swept flying wing

Swept flying wing aerodynamics presents some peculiarities of air-flow in the vicinity of the lifting surface. These are mainly related to the geometric shape in the plan and the main direction of air-flow, which result in reciprocal influence between the two semi-plans which give the median and extreme effects on aerodynamic characteristics (Figure 6).

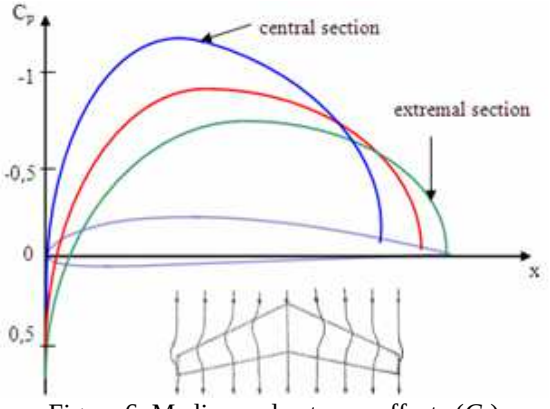

Figure 6. Median and extreme effects (C_p)

The swept wing presents geometrical symmetry and, therefore, some symmetry of the flow. In this case, close to the symmetry plan, the air flows move from each other and widen; in the case of subsonic air flow, according to Bernoulli's law (equations 1 and 2). The result is that, in the central part, this increase of the air path sections will experience a corresponding increase in pressure with a reduction in local flow velocity [11].

$$\frac{v^2}{2g}+\frac{p}{\rho\cdot g}+z=\frac{v_0^2}{2\cdot g}+\frac{p_0}{\rho\cdot g}+z_0 \qquad (1)$$

$$\int\frac{dp}{\rho}+\frac{v^2}{2}+g\cdot z=const \qquad (2)$$

The pressure values are not the same throughout the whole extent of the wing (Figure 6). Thus, in comparison to the pressure variation in a section located halfway in the left or right plan, there is a significant decrease of the basin, especially in the leading wing edge. Eventually there is a substantial increase in the trailing edge.

One of the drawbacks is that, with the increase of the angle of incidence, the flow gets worse sooner than in the case of a straight wing. Due to this, the load-lifting coefficient also starts decreasing earlier and its maximum value (Figure 6) is smaller and reached in incidence angles, which are smaller than the ones of the right wing.

Decreasing the critical angle of incidence and the $C_{z\ max}$ due to premature detachment of the air stream has the following causes:

- **a.** close to the of the wing the real incidence angle becomes larger than in the central area, which makes the boundary layer to be less stable and have a tendency to tear more quickly from the surface of the wing;
- **b.** since the flow is, in part, due to the V_t component, along the span as well, there is considerable thickening of the boundary layer towards the tips of the plans, which favors even more the formation of currents, see Figures 7 and 8.

Based on Figure 8, the following equations can be deduced:

$$V_n=V_\infty\cdot\cos\chi \quad \text{and} \quad \alpha_n=\frac{\alpha}{\cos\chi} \qquad (3)$$

and the lifting is:

$$F_z=\frac{\rho\cdot V_n^2}{2}\cdot S\cdot C_z=\frac{\rho\cdot V_\infty^2}{2}\cdot S\cdot C_z \qquad (4)$$

where $C_z=C_{zn}\cdot\cos^2\chi$.

Similarly

$$F_x = F_{xn} \cdot \cos\chi = \frac{\rho \cdot V_n^2}{2} \cdot S \cdot C_{xn} \cdot \cos\chi \quad (5)$$

$$F_x = \frac{\rho \cdot V_\infty^2}{2} \cdot S \cdot C_x \quad (6)$$

where $C_x = C_{xn} \cdot \cos^3\chi$.

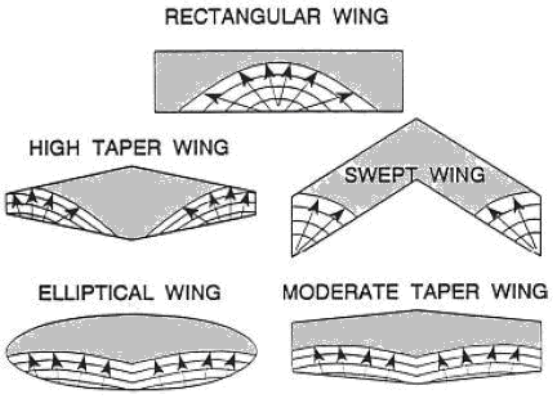

Figure 7. Separation of boundary layer

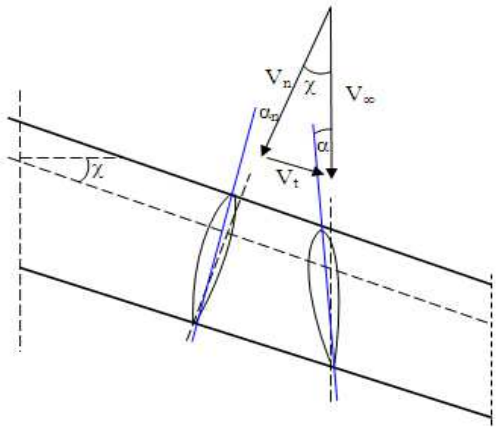

Figure 8. Swept wing speeds

If possible, the following solutions may be adopted, in order to prevent such detachments: curving the wing in such a way as to achieve the reduction of the incidence angle close to the extremity of the wing; the use of profiles that are characterized by critical angles of incidence bigger than those used in the central section; using some slots in leading edge of the wing close to the extremity; mounting aerodynamic knives on the wing's straight back, in the forward direction so as to prevent air slipping, and, therefore, the movement of the boundary layer towards extremities.

Some of the disadvantages are exploited by introducing the concept of twist morphing: low rigidity gives satisfactory morphing amplitude and the control of the detachment of the boundary layer may affect the maneuverability of the flying wing.

3.2. Twist of the swept flying wing

CG emplacement in front of the neutral point does not guarantee the balance; it is only a requirement for longitudinal stability and it is important to obtain stable aerodynamic configurations by using optimal wing twist as well as shape in the plan. According to Nikel [7], the distribution of twist for an optimal lifting coefficient can be established. It has a value between the best glide slope and the best climb rate, and with the selection of C_L wing, the result is $C_{m\,0.25}$. For different profiles for enclosure and at the tip, the average value of C_m of the given aerodynamic profiles is used. The graph in Figure 9 indicates the method for finding the twist angle (β_{req}) by means of elongation values.

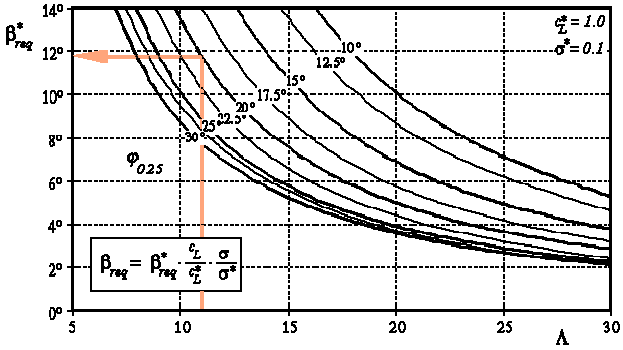

Figure 9. Standard twist angle [7]

The actual inserted twist angle in the graph of Figure 10 is calculated from the standard value. It can be noticed that a reduction of C_L = 0 reduces the required twisting by 50%. Also, if for a lower stability margin (σ), is necessary to have a smaller amount of twist.

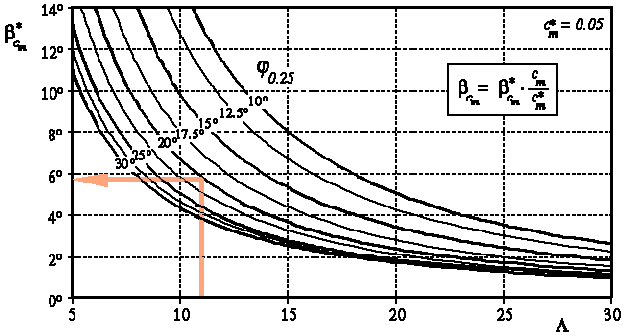

Figure 10. Additional twist angle due to the coefficient of moment [7]

Finally, the geometric twist angle β_{geo} needed to build the wing can be calculated:

$$\beta_{geo} = \beta_{req} - \beta_{\alpha_0} - \beta_{Cm} \quad (7)$$

As numerical application, the input data of Table 1 for the flying wing of Figure 11 is analysed.

Table 1. Flying wing characteristics

Span wing	2.200 m
Root chord	0.400 m
Tip chord	0.200 m
Aspect ratio	7.39
Swept angle at c/4	17°
C_L (coef. lift)	0.5
Root airfoil	Clark YH
Tip airfoil	HS 522
Stability coef.	0.05
Weight	1.8 kg

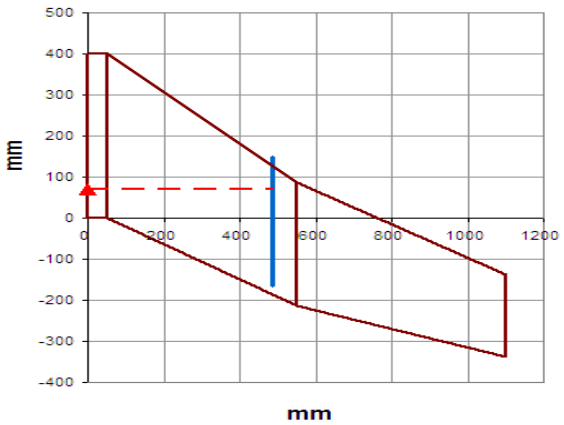

Figure 11. Analyzed flying wing

The characteristics of the enclosure profiles and at the tip are calculated with XFLR5 6.06 and highlighted in Figures 12 and 13 [8, 14].

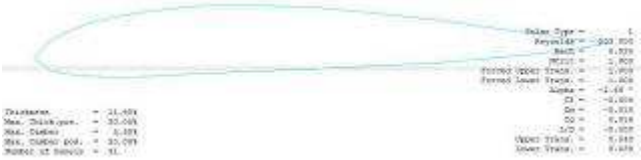

Figure 12. Characteristics of Clark YH

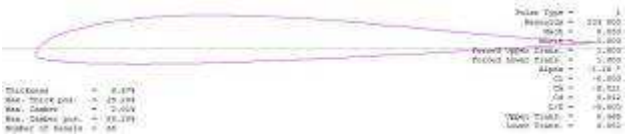

Figure 13. Characteristics of HS 522

In the end, the geometrical twist calculated for the flying wing by means of the above-mentioned algorithm is of 6.9°, while the Panknin [9] is of 7.1°.

3.3. Aerodynamic analysis of constructive twist

Authors suggest the aerodynamic analysis using the XFLR5 6.06 software of the flying wing from figure 11 according to the input data of Table 2 and the chart in Figure 14. The analysis shall be carried out for evolutions with the flight controls locked under standard atmospheric conditions [7].

Table 2. Input data

Speed	10 m/s
Incidence angle	0 ...10°
Twist angle	0° / -7°

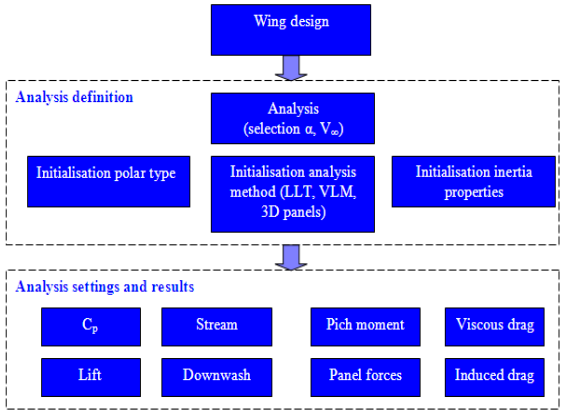

Figure 14. XFLR5 analysis chart

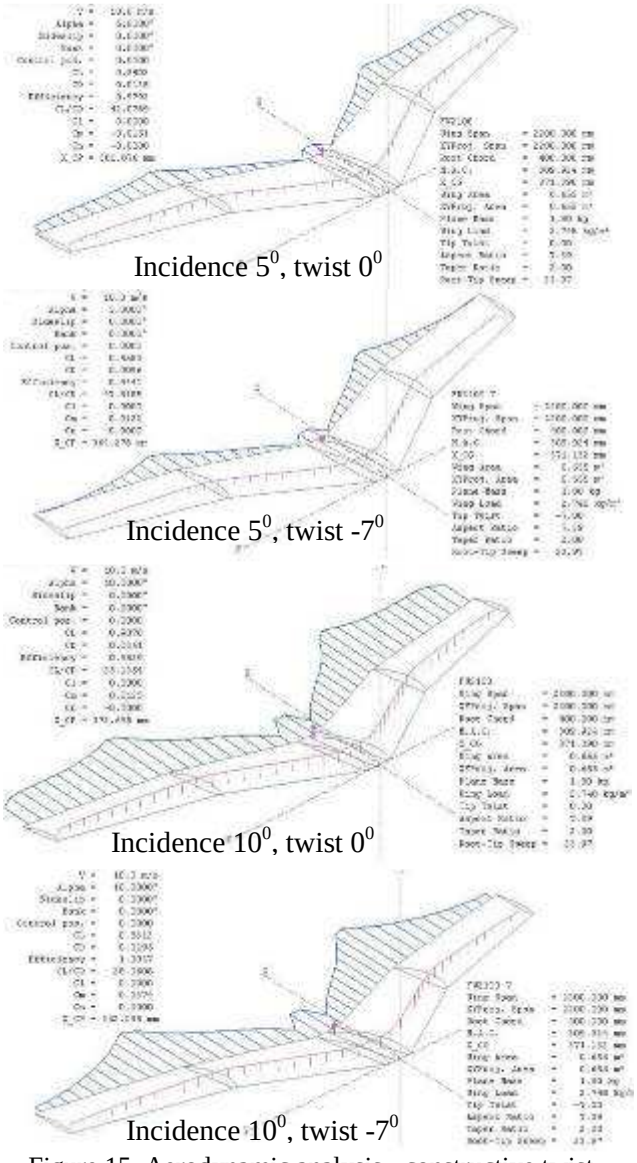

Figure 15. Aerodynamic analysis - constructive twist

As shown in Figure 15, there is an improvement in flight performance in the case of extreme twist of -7° by decreasing induced resistance to the plan ends and increasing the aerodynamic fineness C_l/C_d (see Table 3).

Table 3. Output data

Features	α = 5°		α = 10°	
Twist	0°	-7°	0°	-7°
C_L	0.54	0.45	0.90	0.83
C_m	-0.015	0.012	0.012	0.037
C_L/C_D	42.07	47.81	25.13	28.06

By introducing the corresponding negative twist at the plan ends, higher longitudinal stability values in incidence areas of 5°-10° are obtained (see Figure 16).

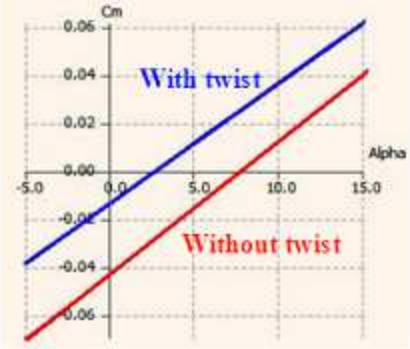

Figure 16. C_m variation according to incidence

Another positive aspect of extreme twist is the release of aerodynamic forces and the decrease of the pressure coefficient Cp of extreme twist areas, shown in Figure 17, the force vectors being obtained at a flying speed of 10 m/s and at an angle of incidence of 5°.

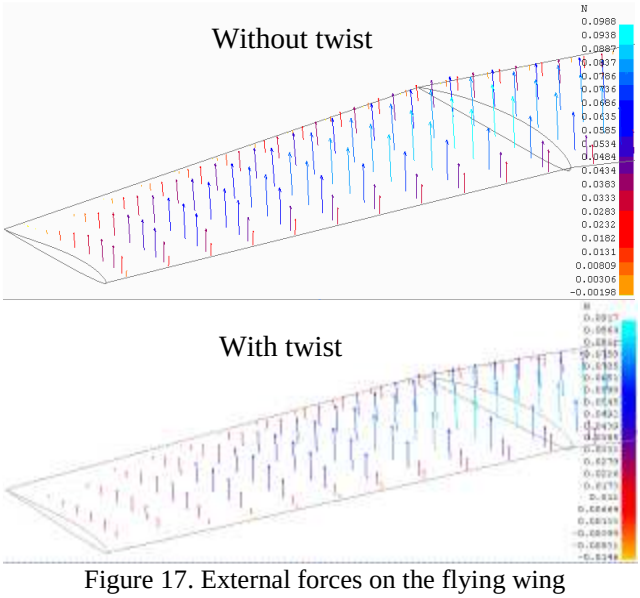

Figure 17. External forces on the flying wing

Induced angle variation is distributed variably over the span according to the incidence angle, see Figure 18.

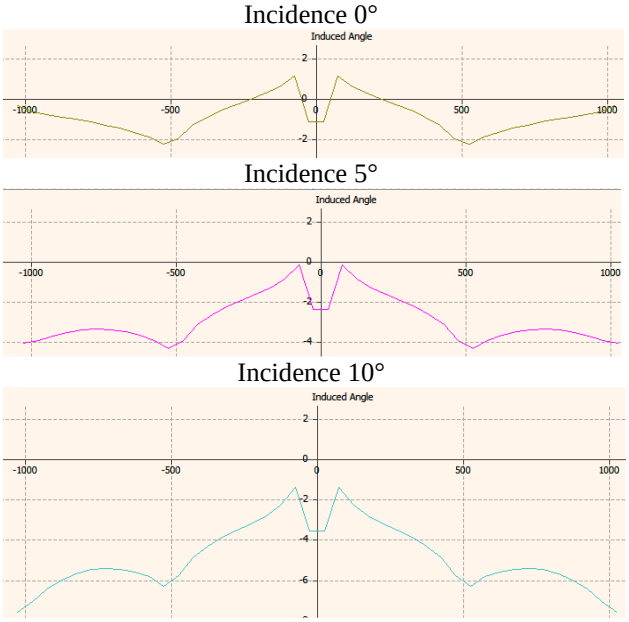

Figure 18. Induced angle variation graph

Due to the air-flow from the lower side of the wing to the upper side of the wing and the occurrence of swirls winglets must be mounted to reduce induced resistance and, thereby, increase flight performance (see Figure 19).

4. Morphing flying wing

4.1. Flying wing geometry

In the preceding paragraphs was demonstrated the need for constructive twist at plan ends, which can be exploited to control the flying wing along 3D trajectories, if the twist angles exceed certain limits. Within the same geometry, a twist-morphing concept based on a semi-flexible extreme structure is proposed which can be modified with the help of servomotors involving a twist bar joint to the extreme rib (see Figure 20). For command and control along the trajectory, the plan ends can twist in a differentiated manner (aileron command) or simultaneously in the same direction (elevator command).

The structure of the flying wing is active aero-elastic on the morphing area and composed of ribs, tubular spars made of composite material and semi-flexible coating, which enables an active angle of approximately ±20°, measured at the extreme rib, see Figure 21. The morphing structure at the ends of the plan is mounted on the fixed wing through reinforced ribs made of lightweight materials and it

includes Futaba action elements of S3003 standard actuators [10].

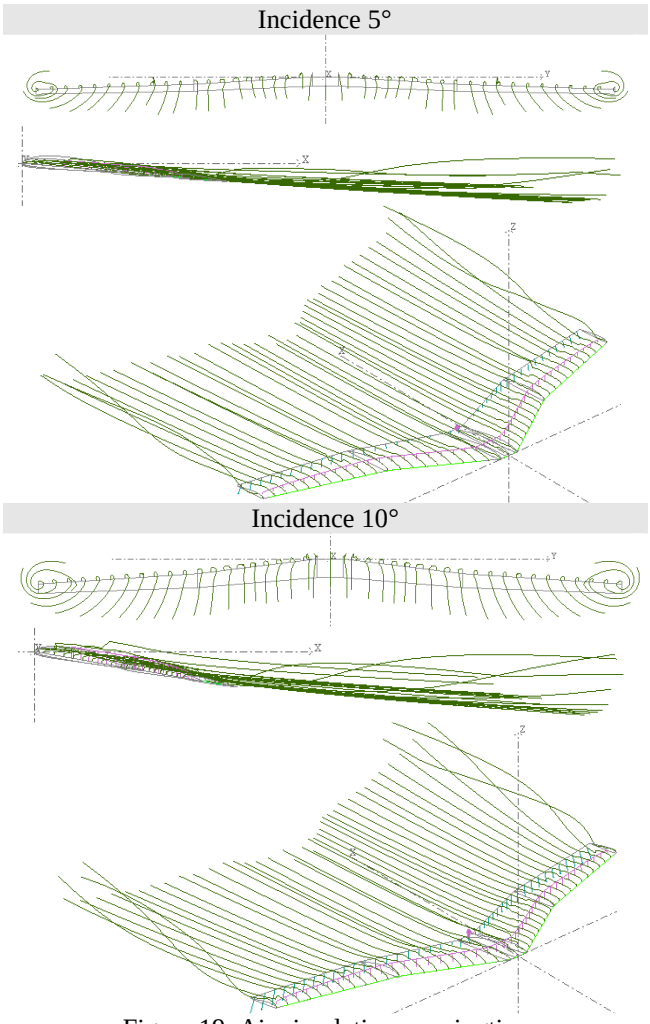

Figure 19. Air circulation on wingtips

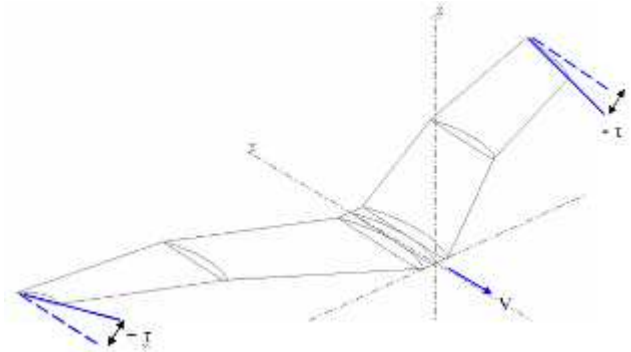

Figure 20. Flying wing design with twist morphing

Figure 21. Flying wing structure

4.2. Comparative aerodynamic analysis of the flying wing

The analysis of the alternative twist on plan ends (alternative morphing) and the aileron command is executed according to the input data in Table 4. Figure 22 shows the evidence of induced resistance while the aerodynamic characteristics are highlighted in Table 4.

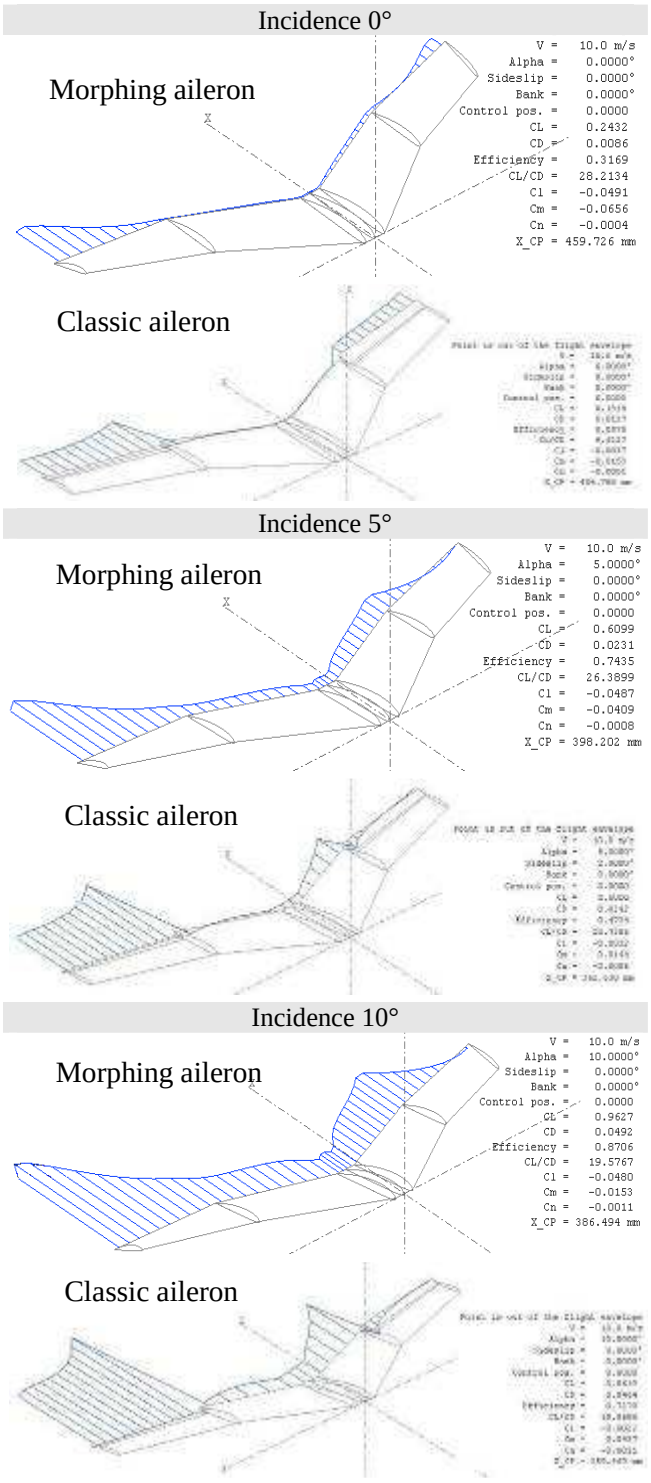

Figure 22. Evidence of induced resistance

Table 4. Input data

Speed	10 m/s
Morphing angle	±15°
Aileron angle	±15°
Incidence angle	0°/5°/10°

Figure 23 is highlights the flow at the ends of the plan in the case of asymmetrical twist (aileron command).

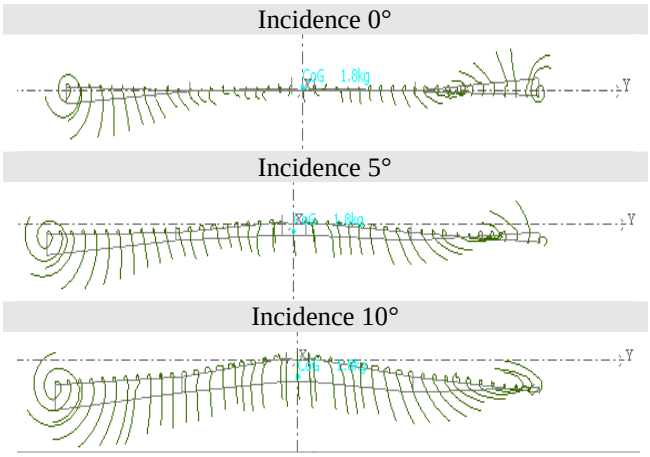

Figure 23. Flow at the ends of the plan

The graph in Figure 24 shows the induced resistance coefficient drag variation (ICD) depending on the incidence.

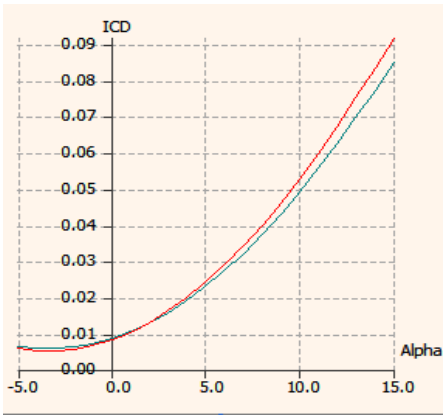

Figure 24. ICD-α graph

For edification of the comparative analysis, is also included the graph of total resistance (Figure 25) as well as the lifting curve (Figure 26) along the span at a speed of 10 m/s and an incidence of 10°.

Analyzing the wing, within the two configurations (classical ailerons, morphing ailerons), in Figures 22, 23, 25 and 26 one can notice a considerable increase of the values of induced resistance, of the total resistance and of the lifting in the lateral area of the ailerons located towards the axis of symmetry, which is due to the formation of swirls with consequences for aerodynamic performance (see Table 5).

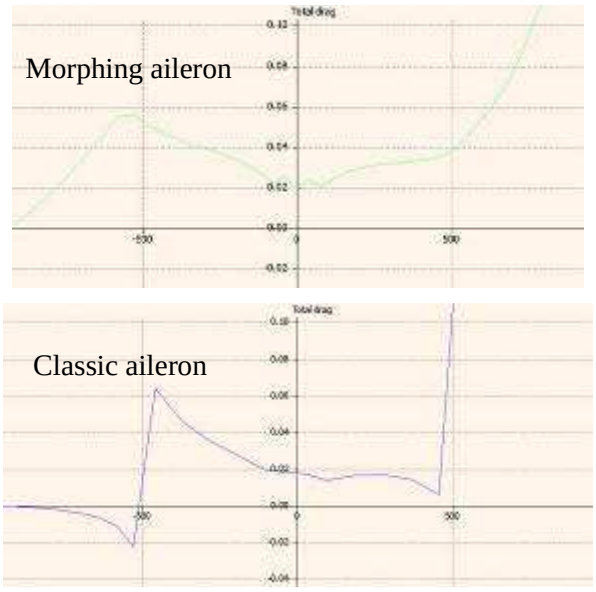

Figure 25. Total drag

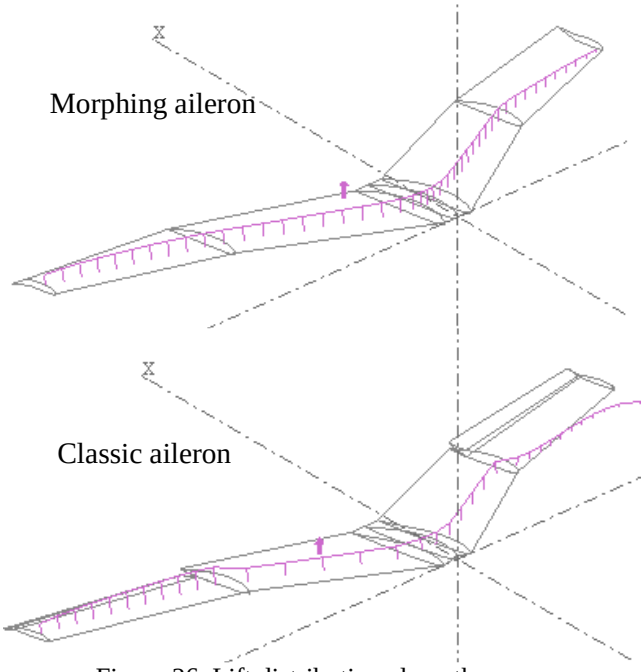

Figure 26. Lift distribution along the span

Table 5. Aerodynamic characteristics in the case of asymmetric twist morphing

	α=0⁰		α=5⁰		α=10⁰	
Control	Morph	Classical	Morph	Classical	Morph	Classical
C_L (lift)	0,240	0,130	0,610	0,510	0,960	0,860
C_D (drag)	0,086	0,01	0,024	0,023	0,049	0,046
C_m (pitch)	-0,06	-0,015	-0,04	-0,014	-0,01	-0,043
C_n (yaw)	-0,0004	0	-0,0008	0	-0,0011	0,001
C_l (roll)	-0,0491	-0,0837	-0,0487	-0,0832	-0,0480	-0,0822

5. Conclusion

The XFLR5 [8, 14] analysis software leads to high reliability results due to the setup options (Reynolds no, no. of iterations, precision factor, limited conditions) and the methods for calculating aircraft performance (LLT-lifting line theory, vortex-lattice method VLM and 3D panel) [15].

The analysed morphing offers, in the case of simultaneous lock (elevator) and of alternate lock (aileron), a command degree sufficient for carrying out flight maneuvers, although, from a constructive point of view, there are negative values of the twist angles of ends of the plan. However, in the given circumstances it is advisable to increase the average steering angles of the surfaces for morphing to obtain 3D maneuvers of the flying wing.

Generally speaking, the solutions are analyzed and compared according to a global indicator based on controllability and aggressive maneuvering. Low manufacturing costs are as important in selecting the morphing strategy.

Acknowledgments

The authors wish to thank the Transilvania University of Brasov and "Henri Coandă" Air Force Academy of Braşov for supporting the research necessary for writing this article.

References

1. O'Grady, B. (2010) *Multi-Objective Optimization of a Three Cell Morphing Wing Substructure*. University of Dayton, USA
2. Galantai, V.P. (2010) *Design and Analysis of Morphing Wing for Unmanned Aerial Vehicles*. Ph.D. thesis, University of Toronto, Department of Mechanical and Industrial Engineering, Canada
3. www.earlyaviators.com/evuia1.htm. Accessed at 09.01 2014
4. Wiggins, L.D., Stubbs, M.D., Johnston, C.O., Robertshaw, H.H., Reinholtz, C.F., Inman, D.J. (2004) *A Design and Analysis of a Morphing Hyper-Elliptic Cambered Span (HECS) Wing*. 45th AIAA/ASME/ASCE/AHS/ASC Structures, Structural Dynamics & Materials Conference, 19-22 April 2004, Palm Springs, California, US, AIAA 2004-1885
5. Hinshaw, T.L. (2009) *Analysis and Design of a Morphing Wing Tip using Multicellular Flexible Matrix Composite Adaptive Skins*. Ph.D. thesis, Virginia Polytechnic Institute and State University, USA
6. Salichon, M. (2009) *Learning Based Methods Applied to the MAV Control Problem*. Ph.D. thesis, Oregon State University, USA
7. Nickel, K., Wohlfahrt, M. (1990) *Schwanzlose Flugzeuge*. Birkhäuser Verlag, ISBN 3-7643-2502-X; available in english as *Tailless Aircraft in Theory and Practice*, AIAA Education Series, ISBN 1-563-47094-2
8. *** (2011) *Guidelines for XFLR5 v6.03*. Available at www.sourceforge.net/projects/xflr5/files/. Accessed at 18.12.2014
9. Hope, G., Kennell, C. (2004) *Logistics Enabler for Distributed Forces*. Technical Report, NSWCCD-20-TR–2004/07, 2004, Naval Surface Warfare Center. Available at: www.dtic.mil/dtic/tr/fulltext/u2/a476380.pdf. Accessed at 23 12.2013
10. *** (2005) *Instruction manual for Futaba 6 EXAP, 6-channel*. PCM / PPM (FM) selectable Radio control system for aircraft, www.futaba-rc.com, accessed at 08.01.2014
11. Houghton, E.L., Carpenter, P.W. (2003) *Aerodynamics for Engineering Students*. Fifth Edition, ISBN 0 7506 5111 3
12. Lazos, B.S., Visser, K.D. (2006) *Aerodynamic Comparison of Hyper-Elliptic Chambered Span (HECS) Wings with Conventional Configuration*. AIAA-2006-3469, 25th AIAA Applied Aerodynamics Conference, San Francisco, CA, US
13. Neal, D.A. (2006) *Design, Development, and Analysis of a Morphing Aircraft Model for Wind Tunnel Experimentation*. Ph.D. thesis, Virginia, USA
14. Katz, J., Plotkin, A. (2011) *Low speed aerodinamics*. Second edition, Cambridge University Press, ISBN-10: 0521665523
15. Demasi, L. (2004) *Aerodynamic Analysis of Non-conventional Wing Configurations for Aeroelastic Applications*. Ph.D. thesis, Politecnico di Torino, Italy

Received in February 2014